AIAA JOURNAL
Vol. 32, No. 9, September 1994

Boundary-Layer Transition Detection with Infrared Imaging Emphasizing Cryogenic Applications

Ehud Gartenberg*
Old Dominion University, Norfolk, Virginia 23529
and
Robert E. Wright†
NASA Langley Research Center, Hampton, Virginia 23681

This paper reviews the technique of boundary-layer transition detection using infrared (IR) imaging, emphasizing cryogenic wind-tunnel testing. With the exception of the low-temperature effects on the IR radiation, the discussion is relevant to conventional wind-tunnel and flight testing as well. At low temperatures, IR imaging encounters a reduction in the radiated energy throughout the IR spectrum, combined with a shift to longer wavelengths of the bulk of the radiation. This radiation behavior affects the minimum resolvable temperature difference (MRTD) of the IR imaging system because of its fixed wave band sensitivity. In the absence of commercial long wavelength IR imaging systems, operating at wavelengths longer than 13 μm, some measures can be taken to alleviate the problem caused by the MRTD limitation. The thermal signature of transition can be enhanced by allowing a small and controlled temperature increase of the wind-tunnel flow that induces a transient heat transfer to the model. This action temporarily reveals the model area under the turbulent regime through its higher heating rate compared with the laminar regime. The contrast between the areas exposed to the two regimes can be enhanced by subtraction of thermograms (the equilibrium thermogram from the transient thermogram). Further visual improvement can be obtained through shade stretching or binary shading.

Nomenclature

A = detector area
c = speed of light
D^* = detectivity of IR detector
e = emissive power
h = Planck constant
i = in-band detectable blackbody radiance, w/m^2 sr
k = Boltzmann constant
M = Mach number
MRTD = minimum resolvable temperature difference at 50% signal modulation, see also appendix A
N = photon emission number
NEP = noise equivalent power of detector
n = refraction index, c_0/c
P = Prandtl number
$\mathcal{P}$ = IR incident power at detector
p = IR detectable power at detector
R = Reynolds number
S/N = signal-to-noise ratio
T = temperature
t = time
U = velocity
x = local coordinate, or unit length
α = angle of attack, or thermal diffusivity
γ = specific heats ratio
Δf = amplifier bandwidth
δ = velocity boundary-layer thickness
ϵ = emittance
λ = wavelength, or spectral property (subscript)
μ = viscosity, or micro (10^{-6})
ν = kinematic viscosity, μ/ρ
ρ = density
σ = Stefan-Boltzmann constant
τ = transmittance, or imager optics transmission
ω = acceptance solid angle, sr

Subscripts

aw = adiabatic wall
b = blackbody
c = chord
r = recovery value in the boundary layer
ref = temperature reference conditions, 303 K
t = total property
$t - l$ = difference between turbulent and laminar values
0 = vacuum conditions
∞ = freestream value

Received Jan. 13, 1992; revision received Dec. 22, 1993; accepted for publication March 4, 1994.

*Research Associate Professor, Department of Mechanical Engineering. Senior Member AIAA.
†Aerospace Technologist, Aerodynamic Measurement Branch, Experimental Testing Technology Division, MS 234.

Introduction

INFRARED (IR) imaging is currently the preferred visualization technique for detection of boundary-layer transition to turbulence, be it in wind-tunnel or flight testing.[1] However, data obtained in conventional wind tunnels are usually not directly applicable to full-scale designs because the viscous effects of the flow as they occur in flight have not been duplicated on scaled models. This discrepancy is known as the "Reynolds number gap" between the flow around a model in the wind tunnel and the flow around an airplane in flight. The plans to develop medium and large transonic transport airplanes with partially laminar flow wings further underlines the problem of the Reynolds number gap, as conventional wind-tunnel testing cannot provide the correct location of the boundary-layer transition, an essential item for accurate drag estimate. The need for high-Reynolds-number wind-tunnel testing was answered by building cryogenic wind tunnels capable of generating flows in which the models' Reynolds numbers match the values encountered by airplanes in flight. These pressurized, closed-circuit wind tunnels operate on the principle of continuous injection of liquid nitrogen into the flow. The vaporization and enthalpy increase of the injected nitrogen absorb the heat generated by the flow friction with the walls, the excess of fluid mass being vented to the atmosphere to keep the flow at the prescribed test conditions. The combination of low flow temperatures, down to 100 K, with moder-

ate pressurization generates, at transonic speeds, Reynolds numbers in excess of 3×10^8 per meter. At constant Mach number, the increase in the Reynolds number with decreasing flow temperature is caused by a decrease of the viscosity and an increase in the density of the flow. Further increase in the Reynolds number is generated by increasing the pressure, thereby increasing the flow density. It should be noticed that in parallel with these changes, the flow velocity at a fixed Mach number decreases with decreasing flow temperature because of the speed of sound dependence on the fluid temperature. Overall, the Reynolds number varies as $T^{-1.4}$ and linearly with pressure. For example, decreasing the temperature from 300 to 100 K and increasing the pressure from 1 to 8 atm increase the unit length Reynolds number ($R/x = \rho U/\mu$) about 37 times.

The IR imaging technique has in principle the right attributes for detection of boundary-layer transition in cryogenic wind-tunnel testing: it is nonintrusive, provides a global picture of the boundary-layer regimes over the wing, does not require repeated surface preparations, and has a relatively fast response. These attributes offer increased wind-tunnel productivity for laminar-flow testing. The use of this technique in cryogenic wind tunnels is similar to its use in conventional tunnels, except that it also has to address the influence of the low temperature on the IR radiation. On the other hand, cryogenic tunnels have the advantage of being operated under continuous temperature control, which provides the option of producing small and controlled heat fluxes on the model. This option enhances the thermal signature of the transition on the model, without altering the natural instability modes of the boundary layer. Therefore, the successful implementation of this technique at the operational temperatures of cryogenic tunnels requires an understanding of the physical laws that govern this application. In a previous paper, Gartenberg et al.[2] reported a feasibility experiment run in the 0.3-M Transonic Cryogenic Tunnel (0.3-M TCT) at NASA Langley Research Center, in which transition was detected down to 170 K with a commercial IR imaging system that operates in the 8- to 12-μm wave band. In this paper, we take a broader look at boundary-layer transition detection with IR imaging at low temperatures. We examine the physics, propose solutions, and sketch directions for future improvements to render this technique fully compatible with the operational conditions in cryogenic wind tunnels. With the exception of the temperature effect on the spectral properties of IR radiation, the discussion of the technique is fully applicable to conventional wind-tunnel testing. It is also relevant to flight testing, where the ambient temperature can be as low as 217 K at cruise altitudes above 11,000 m.

Technique

The detection of laminar boundary-layer transition to turbulence with IR imaging became feasible once the sensitivity required to capture the difference between the adiabatic wall temperatures of the two regimes became technologically available. The value of the adiabatic wall temperature under the turbulent regime being higher compared to the laminar regime, the IR imaging technique indicates the transition region by detecting its characteristic wall temperature increase. The minimum resolvable temperature difference (MRTD) of current IR imaging systems ranges between 0.02–0.1 K, based on blackbody radiation at ambient temperature. Accumulating experience, it was observed that the natural flow heating in closed-circuit wind tunnels enhances the thermal contrast of the transition on the model's surface, through the higher heat flux and surface temperature rise that distinguishes the turbulent from the laminar regime. Thus, in the general case, the spatial and temporal surface temperature distribution is a result of the convective heat exchange between the flow and the model, coupled with the substrate involvement by conduction. Finally, the thermogram of the model as produced by the IR imaging system is determined by the surface temperature distribution, the spectral and directional emittance of the model's surface, the wind-tunnel windows transmittance, and the IR imaging system response.[3] The higher the IR imaging system sensitivity, the lower the Mach number to which this technique could be extended. The following sections analyze the influence of these and other factors on the capability of IR imaging systems to detect transition in conventional and cryogenic wind tunnels.

Working Fluid

The volumetric composition of dry air is approximately 78% N_2, 21% O_2, plus smaller amounts of CO_2, Ar, etc. The atmosphere also contains variable amounts of water vapor that can be as high as 7% at 313 K and 100% relative humidity. Relating to the operating principles of cryogenic wind tunnels, it is apparent that the fluid in these tunnels becomes 100% nitrogen soon after starting their operation. At low temperatures the nitrogen shows some real-gas effects, e.g., a decrease in the turbulent recovery temperature by a few percent,[4] but these effects do not change significantly conclusions inferred from ideal-gas analysis. Therefore, unless otherwise indicated, the analysis in this paper is based on the properties of air, treated as an ideal gas.

The analysis starts with the variation of the recovery temperature in the boundary layer, or adiabatic wall temperature. As mentioned, this is the primary effect acting on a model surface that is in thermal equilibrium with the flow. Considering for simplicity the flat plate case, the difference in the recovery temperatures between areas of turbulent and laminar regimes in the boundary layer is given by

$$\Delta T_{r,\,t-l} = \frac{T_t(\sqrt[3]{P} - \sqrt[3]{P})}{1 + [(\gamma - 1)/2]M_\infty^2}\left(\frac{\gamma - 1}{2} M_\infty^2\right) \tag{1}$$

Equation (1) is also used to estimate $T_{r,\,t-l}$ for airfoils, in which case the freestream Mach number M_∞ is replaced by the local Mach number M at the edge of the boundary layer. Figure 1 shows some plots of Eq. (1) for various total flow temperatures between 300 and 100 K. Notice that $T_{r,\,t-l}$ is linearly dependent on T_t, and therefore at transonic Mach numbers its value decreases from roughly 3 K to roughly 1 K when the test conditions drop from ambient to typical cryogenic conditions. This result is significant because, as will be shown, the IR camera loses sensitivity with decreasing target temperatures.

Nitrogen at low-to-moderate temperatures and pressures can be considered transparent throughout the IR spectrum.[5]

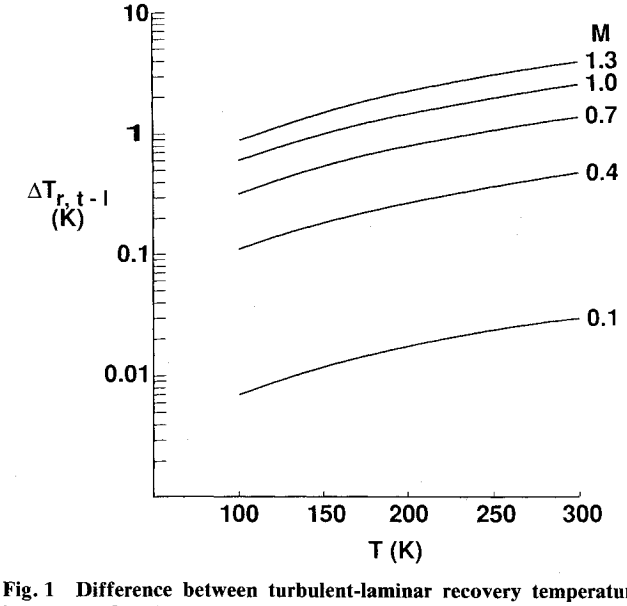

Fig. 1 Difference between turbulent-laminar recovery temperature in the boundary layer as a function of the total flow temperature, for different local Mach numbers.

Gaseous nitrogen does not absorb or emit significant levels of IR energy through vibration-rotation bands because its symmetrical diatomic molecule has no electric dipole moment. Second-order effects of radiation participation appear only at higher pressures (tens of atmospheres), when molecular collisions may produce momentary magnetic dipoles. In the present case, cryogenic wind tunnels operate at pressures below 10 atm, and this effect can be ignored. Compared with air transmittance of IR radiation, pure nitrogen has the advantage of being free of the absorption bands of carbon dioxide and water vapor.

IR Radiation at Low Temperatures

The IR monochromatic emissive power $e_{b,\lambda}(T)$ of a perfect emitter "blackbody" is described by Planck's law as

$$e_{b,\lambda}(T) = \frac{2\pi hc_0^2}{\lambda^5[\exp(hc_0/\lambda kT) - 1]} \tag{2}$$

where the refraction index of the surrounding medium $n = 1$. Planck's law gives the spectral emissive power of a blackbody as a function of the radiation wavelength for a given temperature. A family of such log-log "Planckian curves" is shown in Fig. 2. For presentation convenience, the ordinate was tilted to bring the maxima of the individual curves one underneath the other. The total emissive power available from a blackbody at a given temperature is obtained by integrating Eq. (2) over the entire wavelength spectrum. This integral can be worked in closed analytical form

$$\int_0^\infty e_{b,\lambda}(T)\, d\lambda = \int_0^\infty \frac{2\pi hc_0^2}{\lambda^5[\exp(hc_0/\lambda kT) - 1]}\, d\lambda = \sigma T^4 \tag{3}$$

which is known as the Stefan-Boltzmann equation. This elegant result yields the total power radiated by a blackbody surface at a given temperature, and it is useful for overall radiative heat transfer calculations. However, only the spectral characteristics of IR radiation and of the specific IR system in use can provide the necessary information to analyze a particular application. Planck's law indicates that spectral emissive power of IR radiation peaks at

$$\lambda_{e_{b,\lambda_{max}}}(\mu m) = 2898/T(K) \tag{4}$$

this relationship being known as Wien's displacement law. For example, the IR radiation of a body at 300 K peaks at 9.7 μm, whereas at 100 K it peaks at 29.0 μm. Furthermore, the behavior of the Plankian function indicates that at any temperature 75% of the total IR energy emitted from a blackbody is radiated at wavelengths beyond $\lambda_{e_{b,\lambda_{max}}}$, i.e.,

$$\int_{\lambda_{e_{b,\lambda_{max}}}}^\infty e_{b,\lambda}\, d\lambda = 0.75\sigma T^4 \tag{5}$$

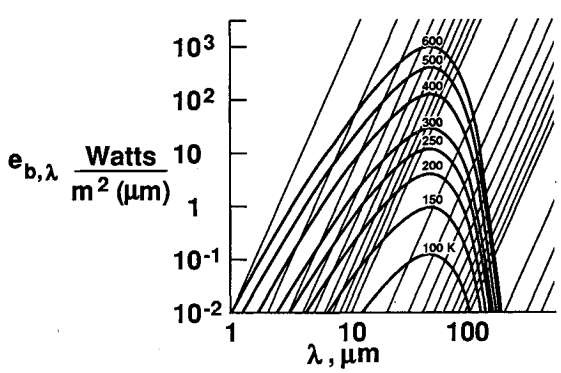

Fig. 2 Planckian curves of spectral radiant power, for different blackbody temperatures.

Equations (4) and (5) indicate that with decreasing target temperature, the bulk of its IR radiation is emitted at ever-increasing wavelengths. Hence, for applications of IR imaging at low temperatures, there is a demonstrated incentive to operate at the longest wavelengths of existing IR sensors and optics.

Before closing this section, attention is drawn to the fact that most detectors used in IR imaging systems are photon sensors, as opposed to radiation energy sensors. By dividing both sides of Planck's law, Eq. (2), by the energy of a single photon hc_0/λ, one obtains the blackbody spectral photon emission number

$$N_{b,\lambda} = (\lambda/hc_0)e_{b,\lambda} \tag{6}$$

for which Wien's displacement law becomes

$$\lambda_{N_{b,\lambda_{max}}}(\mu m) = 3663/T(K) \tag{7}$$

Thus, the peak photon emission is displaced farther to longer wavelengths relative to the peak energy emission. For example, at 300 K, the peak photon emission occurs at 12.2 μm compared with the peak energy emission at 9.7 μm; at 100 K, the photon emission peaks at 36.7 μm compared with 29.0 μm for the energy emission. These considerations strengthen the argument favoring long wavelength IR equipment for scanning low-temperature targets.

IR Imager

Commercial IR imaging systems are designed to operate either in the 2- to 5-μm or in the 8- to 12-μm wave bands "atmospheric windows," in which relatively little of the IR radiation is absorbed by the water vapor or the carbon dioxide in the air. The spectral distribution of the IR radiation indicates that the system operating at the longer wavelengths (8 to 12 μm) is more effective for low-temperature applications. Longer wavelength IR imaging systems are not commercially available because of the lack of a sizable market, but recent space and other applications have spurred the development of this technology.

The estimated performance of a commercially available IR imager operating in the 8- to 12-μm wave band (Fig. 3) indicates a deterioration in the MRTD with target temperature. (See the Appendix.) Obviously, for transition detection to be possible, the rise in its adiabatic wall temperature should be greater than twice the IR imager MRTD. Furthermore, the temperature threshold for detection is also determined by the spatial resolution of the IR imager that determines the number of pixels over which the transition region is scanned. A comparison between the MRTD variation with temperature (Fig. 3) and the steady-state thermal signature of boundary-layer transition on a transonic airfoil, $T_{aw,t-l}$ or $T_{r,t-l}$ (Fig. 1), shows that the values of the two parameters become approximately equal around 250 K. As flow and target temperatures

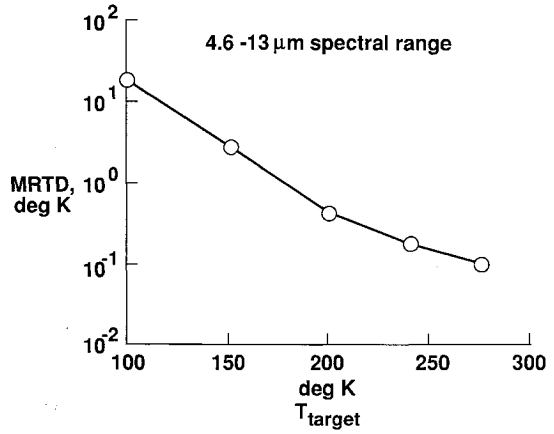

Fig. 3 Estimated sensitivity of a commercially available IR imaging system equipped with a mercury-cadmium-telluride (HgCdTe) detector.

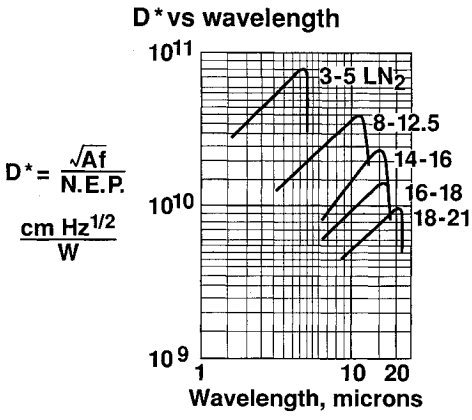

Fig. 4 Performance of a family of mercury-cadmium-telluride (HgCdTe) detectors, formulated for different IR wave band sensitivity (InfraRed Associates catalog, Cranbury, NJ 08512).

decrease below 250 K, $T_{aw,t-l}$ continues to decrease linearly, whereas the MRTD increases. These relationships explain the results obtained in the T2 cryogenic wind tunnel at ONERA-CERT by Seraudie et al.,[6] who reported transition detection down to 240 K.

Extending the operating wave band of a given IR imaging system to longer wavelengths is not a trivial problem. First, as shown in Fig. 4, within the same family of detectors those optimized for longer-wavelength sensitivity do so at the expense of decreased sensitivity (the D^* detectivity parameter of IR sensors is defined at the end of this section). Other types of sensors may exhibit a definite peak in sensitivity at a long wavelength, but their inadequate overall performance may render their application to an IR imager impractical. Second, most refractive optical lenses and windows have degraded performance in the extended wave band. Therefore, for the near term, the goal should be to develop test procedures for transition detection in cryogenic tunnels that make the most out of commercial IR imaging systems that operate in the 8- to 12-μm wave band. Eventually, IR imaging systems dedicated to cryogenic wind tunnels, incorporating genuine long wavelength sensors and reflective optics, should be considered.

Referring to Fig. 4, the sensitivity, or detectivity, performance parameter D^* is defined for a detector of 1 cm^2 in area whose noise is reduced to that obtained with an amplifier of 1-Hz bandwidth

$$D^* = \frac{1}{NEP}(\Delta f/A)^{1/2} \tag{8}$$

where the noise equivalent power $NEP = \mathcal{P}/(S/N)$.

Wind-Tunnel Models

The majority of models built for cryogenic wind-tunnel testing are fabricated from steel or aluminum alloys specifically certified for this kind of operation.[7] In the 0.3-M TCT, testing was done also with airfoils made of a steel spar wrapped in a fiberglass-epoxy skin. Both manufacturing options meet the extremely smooth surface finish that is required to prevent triggering early transition. This aspect of cryogenic testing becomes more stringent as the boundary-layer thickness decreases with decreasing flow temperature. To illustrate this constraint, the flat plate laminar boundary-layer thickness is given by

$$\delta(x) = 5.0x^{1/2}(R/x)^{-1/2} \tag{9}$$

At constant Mach number, the Reynolds number dependency on temperature is approximately proportional to $T^{-1.4}$. Therefore, the boundary-layer thickness at the upper limit of the Reynolds number conditions (say, 100 K and 8 atm) can be thinner by a factor of 6 than at ambient conditions. When the resulting surface quality criterion is applied to metallic models, it indicates the need to polish their surfaces close to mirror finish, which in turn produces low emittance and high reflectance. These conditions make metallic models difficult targets for infrared imaging measurements, because they reflect energy from the surroundings and emit little energy to be detected. Figure 5 shows the directional emittance of a few metals, the behavior of steel being very much similar. Consequently, IR thermograms of polished metallic models have very low signal-to-noise ratios.

Another feature of metallic models is their high thermal capacity, conductivity, and diffusivity that attenuate the surface thermal signature of transition through longitudinal and in-depth heat conduction. Under the worst conditions, the surface temperature distribution drops below the IR imager's MRTD, rendering transition detection impossible. At low temperatures this problem worsens, as the thermal conductivity of most metals varies inversely proportional with the temperature. For some steels, for example, the conductivity at 100 K is 50% higher than at 300 K.

These facts suggest that models made of composite materials, or having composite skins, are more desirable for IR testing than polished metallic models. There are several reasons to favor composite-made fiberglass models. First, their emittance is higher compared with metallic models. Typically, the emittance of the epoxy coating of fiberglass fabric is better than 0.9, as compared with values below 0.1 for polished metallic models. On the contrary, the reflectance, whose contribution to the thermograms is all noise, is complimentary to the absorptance and hence to the emittance, and assumes low values, usually below 0.1. This explains the significantly higher signal-to-noise ratios of thermograms of composite models compared with thermograms of metallic models. Next to be considered is the thermal conductivity aspect. At 300 K, the typical thermal conductivity of steels ranges between 20 to 60 w/mK, whereas the fiberglass has a typical value of 0.3 w/mK. Therefore the thermal insulator character of composite models helps to preserve the level of the temperature change caused by the transition close to its adiabatic wall values, and to confine it to the location of its occurrence. Furthermore, the decrease in the thermal conductivity of fiberglass with temperature is only beneficial to this application. The factors just discussed are absolutely necessary for a successful implementation of this technique under any test condition. However, at low temperatures and/or low Mach numbers, recourse must be made to the convective heat transfer characteristic of the transition to augment its thermal signature on the model to a level where it becomes detectable by IR imaging systems.

The location of the laminar boundary-layer transition to turbulence is known to be sensitive to nonadiabatic wall effects. Transition data are assumed to refer to adiabatic conditions, unless otherwise indicated. A higher or lower wall temperature relative to the adiabatic wall temperature can affect the boundary-layer stability, thus affecting the transition location. This sensitivity to heat transfer requires that experiments in natural transition be performed under thermal equilibrium

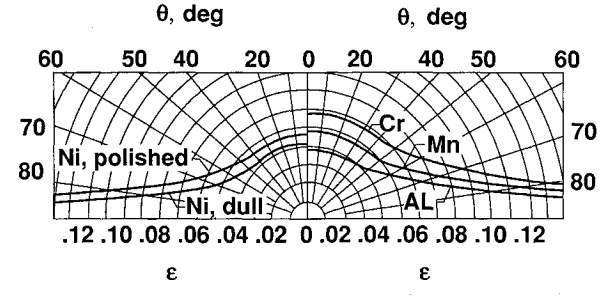

Fig. 5 Distribution of the total directional emittance for several metals (from E. Schmidt and E. Eckert, *Forsch. Gebiete Ingenieurw.*, 6:175, 1935).

conditions between the model and the flow. The apparent contradiction between the thermal equilibrium requirement and the suggestion to use heat transfer effects to detect transition is elaborated in the Solutions section.

IR thermograms may indicate true or false surface temperature variations that can be either unrelated or only partially related to transition. For example, uneven surface emittance can cause a false indication of temperature variation. On the other hand, true temperature variations can be caused either by nonuniform skin thickness, or by a combination of different materials used in the substrate. This is particularly true when the transition signature is enhanced through convective heat transfer. Variations in thickness may occur in both stainless steel and composite skin models, whereas a variation in substrate materials is usually associated with fillers underneath composite skins.

Wind-Tunnel Windows

Infrared transparent windows are available in a variety of materials. Previous testing showed that germanium and zinc-selenide can perform well in the cryogenic environment.[2] The transmittance of the raw material can be enhanced through antireflective coating on both sides of the window, to exceed 0.9. Our experience indicates that these coatings are compatible with the cryogenic wind-tunnel environment. However, as shown in Fig. 6 for zinc-selenide (the same holds true for germanium), this solution cannot extend the effective transmittance of these materials to wavelengths beyond 14 μm, and new materials must be evaluated for long wavelengths applications. The compatibility criteria for these materials are spectral transmittance (including variation with temperature), moduli of rupture, thermal shock resistance, adaptability to antireflective coating, water solubility, size, machining, and cost.

One advantage of the low-temperature environment is the minimization of the windows' self-radiation, a source of possible noise.

Solutions

This discussion of transition detection in cryogenic wind tunnels requires specific attention to each individual factor involved in such an experiment: the IR imaging system, the model, and the testing procedure.

By now it is evident that to maximize the capture of the IR radiation emitted by a model at low temperatures, a compatible IR imaging system, including windows, should operate at long wavelengths, ideally in the 30- to 40-μm wave band. However, because such systems are not commercially available, the interim solution is to use an IR imager operating in the 8- to 12-μm band.

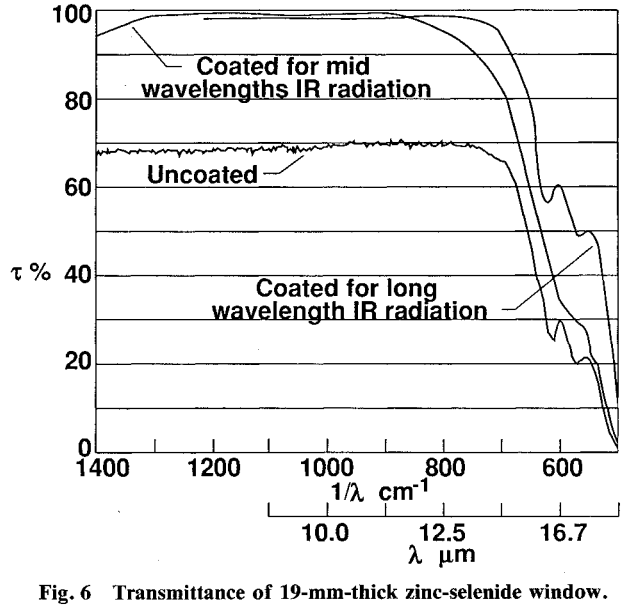

Fig. 6 Transmittance of 19-mm-thick zinc-selenide window.

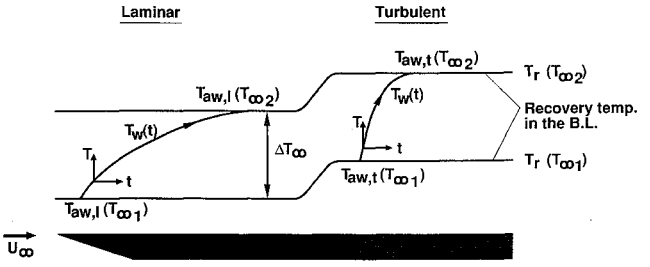

Fig. 7 Schematic description of wall temperature response to a step change in freestream temperature.

Models designated for this application should be fabricated from composite materials, or should have a composite skin. Good experience was accumulated with epoxy-coated fiberglass surfaces that provide an emittance close to blackbody values. The high emittance enhances the surface radiation, attenuates the noise originating from background reflections, and thus increases the signal-to-noise ratio on the thermograms. Compared with metallic models, the thermal conductivity of fiberglass is about two orders of magnitude lower, thus preserving the surface temperature difference caused by boundary-layer transition.

So far the analysis assumed steady flow conditions in the wind tunnel. However, besides the positive difference in the recovery temperature between the turbulent and the laminar regimes, there is also a sharp increase in the value of the convective heat transfer coefficient. This effect is observed when the wall temperature is different from the recovery temperature in the boundary layer and the model exchanges heat with the flow. Therefore, by allowing the flow in the wind tunnel to heat moderately, a transient heat transfer that augments the steady-state thermal signature of the transition is induced at the model surface. This process is depicted schematically in Fig. 7. Starting from steady-state flow and no heat transfer, condition "1," the flow is allowed to heat moderately to temperature "2." As a result, heat transfer between the flow and the model occurs, that area exposed to the turbulent boundary layer heating faster than the area under the laminar regime. Eventually, the model reaches a new thermal equilibrium with the flow at the higher temperature. However, during the thermal transient there comes an instant when the temperature difference between the areas exposed to the two regimes is maximized. A thermogram taken at this instant contains the best thermal contrast indicating the transition location. It can be captured either on videocassette or by digitally storing the thermograms at a frequency that ensures proper sampling of the thermal transient.

To reconcile this thermal transient technique with the need to carry transition experiments under thermal equilibrium conditions, the flow heating should not exceed 1% of its total temperature to prevent interference with the natural stability of the laminar boundary layer.[8] A controlled increase of the flow temperature can easily be performed in cryogenic wind tunnels, where the flow parameters are actively controlled anyway during operation. Therefore, changing or keeping a parameter constant is only a matter of a command to the wind-tunnel control system.

During the transient heat transfer, the insulating characteristics of composite models are again acting to the advantage of the IR imaging technique by preventing the heat flux from dissipating rapidly into the model substrate. Solutions to unsteady heat conduction equations of the type

$$\frac{\partial T}{\partial t} = \alpha \nabla^2 T \tag{10}$$

indicate that the low thermal diffusivity of the fiberglass will better inhibit the heat flux from dissipating into the substrate

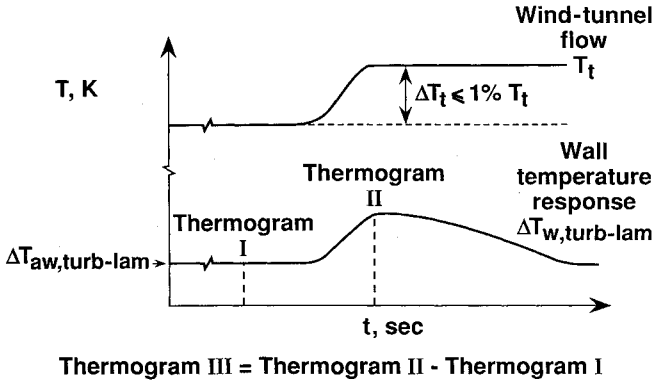

Fig. 8 Methodology for detection of boundary-layer transition in cryogenic wind tunnels by IR imaging.

than the steel (typical $\alpha_{steel} = 10^{-5}$ m^2/s, whereas $\alpha_{fiberglass} = 10^{-7}$ m^2/s). Therefore, as in the case of thermal equilibrium conditions, the transient temperature pattern too will display a sharper spatial contrast on a fiberglass surface compared with a steel surface.

If the thermal transient technique still does not produce satisfactory results, digital image processing can be used to reveal the transition location. An effective method is thermogram subtraction, described in Fig. 8. This method consists of subtracting a steady-state thermogram, taken before the heating of the flow, from the transient thermogram that captured the maximum temperature difference between the turbulent and laminar areas. The subtraction of the steady-state thermogram I from the transient thermogram II decreases the temperature range of the display, and produces a resulting thermogram III where the net temperature effect caused by the flow heating appears very pronounced. This operation also filters out some of the false indications of temperature variations caused by nonuniform surface emittance and background reflections.

The enhancement of thermograms through image processing is justifiable by the objective of this technique, which is satisfied by defining the areas exposed to the two boundary-layer regimes. Further processing options include contouring, filtering, shade stretching, and binary shading. Shade stretching enhances the contrast on the thermograms by making the light areas lighter and the darker areas darker. Binary shading consists of assigning one shade (say dark) to the surface temperatures under the laminar regime and another shade (say light) for the turbulent regime.

Compatibility with Microthin Deposited Hot Films

A complete analysis of experimental data of laminar boundary-layer transition to turbulence includes the global extent of the laminar flow, the identification of the transition mechanism, and spectral and spatial information on the instability that causes the transition. In theory, there are a number of candidate experimental techniques to produce this information. However, for operational and data quality concerns, the current practice calls for use of IR imaging to obtain the global information and to identify the transition mechanism, and for use of microthin deposited hot films to obtain the spectral information on the instability leading to transition. The microthin deposited hot films were developed specifically to satisfy the surface smoothness requirements of cryogenic testing by restricting the height of the protuberances below the value that triggers transition. In this new technology, the metallic hot films and their leads are vacuum deposited directly on a dielectric surface or coating applied on the model of interest. By a fortuitous coincidence, these dielectric substrates, which are absolutely necessary for the deposition and operation of microthin deposited hot films, also provide the surface heat insulation and high-emittance characteristics that are necessary for transition detection with IR imaging. Therefore, the symbiosis between microthin deposited hot films and IR imaging provides the only combination of global and spectral techniques capable of operating simultaneously on the same surface. The combination of these two techniques also allows mutual real-time verification of the data produced by each individual technique.

Sample Results

In a series of experiments performed in the 0.3-M TCT, IR imaging was tested for transition detection on three models with distinctly different surfaces on which microthin hot films were deposited: hot films deposited on a thin layer of silica fused on the fiberglass-epoxy skin of an airfoil; hot films etched on metals deposited on a polyimide sheet glued on an aluminum airfoil; and hot films deposited on a thin film of polyimide sprayed on a steel airfoil.

The following brief discussion addresses only the aspects of transition detection by IR imaging on these surfaces, on which microthin deposited hot films were tested too. Results of boundary-layer transition detection with microthin deposited hot films in cryogenic wind tunnels will be reported separately.

The case of transition detection on a fiberglass-epoxy surface was reported in Ref. 2 and was verified a number of times since then. It appears that current 8- to 12-μm IR imagers can detect transition on this kind of surface at total temperatures as low as 180–170 K, provided the tunnel walls, the model, and the flow are in thermal equilibrium.

The case of transition detection on a polyimide sheet glued to a metallic model can be viewed as similar to the case of the fiberglass-epoxy surface. In both cases a polymeric skin is glued to a metallic spar or a metallic model, the main difference being that the polyimide sheet is considerably thinner, approximately 0.18 mm thick. As indicated by Figs. 9 and 10, pronounced signatures of the turbulent boundary layer were obtained at temperatures between 260 and 200 K.

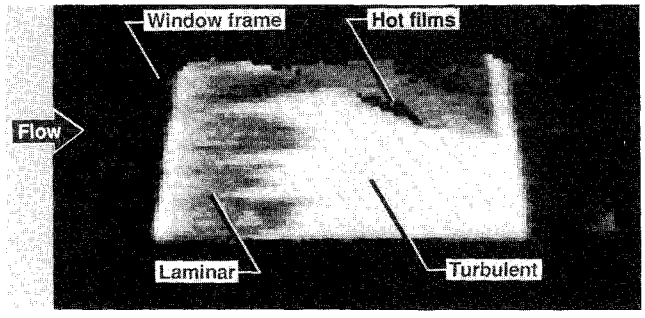

Fig. 9 Transition detection at 260 K by IR imaging and image enhancement on a 6-in. chord SC(2)-0712 airfoil in the 0.3-M Transonic Cryogenic Tunnel. The surface is 0.18-mm polyimide sheet glued on the aluminum model. $T_t = 260$ K, $\Delta T = 3.0$ K, $\alpha = -1.0$ deg, $M_\infty = 0.50$, and $R_c = 2.5 \times 10^6$.

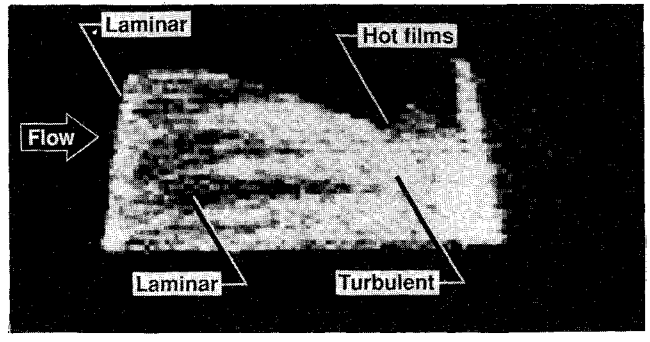

Fig. 10 Transition detection at 200 K by IR imaging and image enhancement on a 6-in. chord SC(2)-0712 airfoil in the 0.3-M Transonic Cryogenic Tunnel. The surface is 0.18-mm polyimide sheet glued on the aluminum model. $T_t = 200$ K, $\Delta T = 2.0$ K, $\alpha = -2.5$ deg, $M_\infty = 0.50$, and $R_c = 3.6 \times 10^6$.

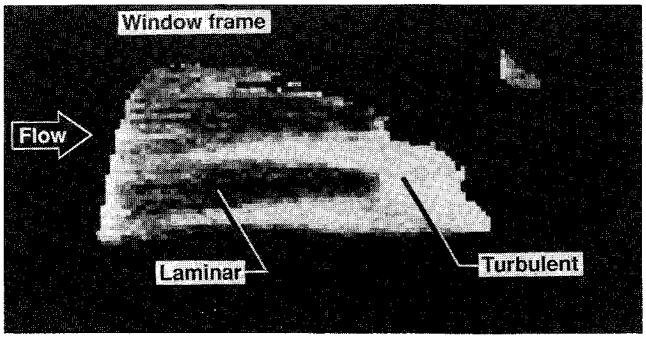

Fig. 11 Transition detection at 270 K by IR imaging and image enhancement on a 6.5-in. chord HSNLF(1)-0213 airfoil in the 0.3-M Transonic Cryogenic Tunnel. The surface is polished aluminum sprayed with polyimide. $T_t = 270$ K, $\Delta T = 3.0$ K, $\alpha = -1.0$ deg, $M_\infty = 0.5$, and $R_c = 3.9 \times 10^6$.

Most wind-tunnel tests are performed on metallic models, and there is interest in transition detection on such models. The surface of such a model was sprayed with polyimide, as a preparatory step to hot-film deposition, and tested for IR transition detection at 270 K with good results, as indicated by Fig. 11. This method has probably a more limited temperature range of usefulness because of the higher rate of heat dissipation into the metallic model through the very thin polyimide film. Even though 270 K is closer to ambient than to cryogenic temperatures, this result is reported herein because of its quality and significance.

The evidence produced by the experiments performed on the fiberglass-epoxy models indicates that dedicated long wavelength IR imaging systems can extend the usefulness of this transition detection technique to the entire range of operational temperatures in cryogenic wind tunnels. The experiment performed on a metallic model sprayed with polyimide indicates that reliable detection of transition is possible on such models at ambient conditions. Long wavelength IR imaging systems are likely to extend this capability to lower temperatures.

Conclusions

Analysis and experimental investigation of boundary-layer transition detection with IR imaging in cryogenic wind tunnels indicate that with proper procedure and attention to details this technique can be successfully used. The main characteristic of this application is the decrease of the IR radiation level at low temperatures that is accompanied by a simultaneous shift of the bulk of the emission to longer wavelengths. Commercial IR imagers are designed to scan targets at ambient or higher temperatures. Extending their use to low-temperature targets has to take into consideration a sensitivity deterioration that is caused by their operation at shorter than optimal wavelengths. Therefore, the successful implementation of this technique in cryogenic wind tunnels requires a testing procedure that maximizes the contribution of each component of the experimental setup to the task at hand. It was shown that among commercial IR imagers, those operating in the 8- to 12-μm wave band come closest to meeting the requirements of this application. Germanium and zinc-selenide windows proved to be compatible with the cryogenic environment, and antireflective coating can improve their transmittance beyond 90% in the imager wave band. Wind-tunnel models with fiberglass-epoxy skin have both the high emittance and the good thermal insulation properties that are critical to produce the IR thermal signature of transition. This signature can be augmented by allowing the flow in the tunnel to heat moderately, thus causing a heat flux into the model. This controlled and moderate heating of the model reveals temporarily the area exposed to the turbulent regime, through its faster heating rate relative to the laminar regime. Finally, image processing through thermogram subtraction and binary shading, or shade stretch, enhances the information on the thermograms by filtering out some of the noise and contrasting between the areas exposed to laminar and turbulent flow.

A model with fiberglass-epoxy skin proved to be the most responsive for this application, allowing transition detection at temperatures as low as 170 K. This was followed by a metallic model with a thin sheet of polyimide glued on its surface, on which transition was detected at temperatures down to 200 K. It was also shown that transition detection is possible on polished metallic models that are sprayed with polyimide.

Eventually, detection of boundary-layer transition over the entire operational range of temperatures of cryogenic tunnels will be performed with dedicated long wavelength IR imaging systems operating in wave bands up to 40 μm, which match the spectral properties of IR radiation at low temperatures.

Appendix: Estimation of an Infrared Imager MRTD

In the absence of low-temperature blackbodies (below 273 K), the MRTD of an IR imager can be estimated under the following assumptions:

1) The MRTD at any temperature is equivalent to a constant amount of power incident on the detector.

2) The following entities are assumed to be constant: target emittance, optical path transmittance, background radiation, atmospheric temperature, and composition.

3) The IR imager is assumed to operate with fixed optics, aperture and filter, which are kept at constant temperature.

Given a measured or manufacturer quoted $\mathrm{MRTD}_{\mathrm{ref}}$, MRTDs at other temperatures can be estimated. The power transfer from a blackbody or other source to the imager detector is given by the standard radiometry equation[9]

$$p = A\epsilon\tau\omega i \tag{A1}$$

For this analysis, blackbody conditions ($\epsilon = 1$) are assumed. The in-band detectable radiance and its rate of change with temperature are calculated for a blackbody source by numerically integrating the product of the relative spectral response of the system (from the system's specifications) times the Planckian radiation distribution, Eq. (2), evaluated at the particular temperature. Thus, the detectable power at the detector changes with temperature as

$$\frac{\mathrm{d}p}{\mathrm{d}T} = A\tau\omega\left(\frac{\mathrm{d}i}{\mathrm{d}T}\right) \tag{A2}$$

and the detectable power at the detector for the target temperature of interest is obtained by multiplying Eq. (A2) by $\mathrm{d}T = \mathrm{MRTD}$:

$$\mathrm{d}p_{\mathrm{MRTD}} = A\tau\omega\left(\frac{\mathrm{d}i}{\mathrm{d}T}\right)\mathrm{MRTD} \tag{A3}$$

where $\mathrm{d}i/\mathrm{d}T$ can be calculated for any temperature and $\mathrm{MRTD}_{\mathrm{ref}}$ is known. Now, $\mathrm{MRTD}_{\mathrm{ref}}$ and $(\mathrm{d}i/\mathrm{d}T)_{\mathrm{ref}}$ can be substituted into Eq. (A3). the estimated MRTD for T is obtained by evaluating Eq. (3) at T_{ref} and dividing it by the same equation evaluated at T.

This procedure is also applicable if filters, apertures, or emittances change between the reference condition and other temperatures. Attenuation of incident energy by internal apertures can be treated as changes in system transmission rather than changes in the acceptance angle. Effects of spectrally selective filters or target emittance can be accounted in the numerical integration of i.

In the present case, presented in Fig. 3, the manufacturer claimed MRTD = 0.07 K at 303 K was used, because testing had verified that the imager MRTD at this temperature was less than 0.1 K, which was the minimum temperature setting step of our blackbody simulator.

Acknowledgment

The first author was supported under NASA Langley Research Center Grant NAS 1-18584-58.

References

[1]Gartenberg, E., and Roberts, A. S., Jr., "Twenty-Five Years of Aerodynamic Research with IR Imaging: A Survey," *Proceedings of Thermosense XIII,* Society of Photo-Optical Instrumentation Engineers, Bellingham, WA, 1991, pp. 338–356; also *Journal of Aircraft,* Vol. 29, No. 2, 1992, pp. 161–171.

[2]Gartenberg, E., Johnson, W. G., Jr., Johnson, C. B., Carraway, D. L., and Wright, R. E., Jr., "Transition Detection Studies in Cryogenic Environment," AIAA Paper 90-3024, Aug. 1990.

[3]Gartenberg, E., and Roberts, A. S., Jr., "Phenomenological Aspects of Infrared Imaging in Aeronautical Research," AIAA Paper 88-4674, Sept. 1988.

[4]Johnson, C. B., and Adcock, J. B., "Measurement of Recovery Temperature on an Airfoil in the Langley 0.3-M Transonic Cryogenic Tunnel," AIAA Paper 81-1062, June 1981.

[5]Sparrow, E. M., and Cess, R. D., *Radiation Heat Transfer,* Hemisphere, Washington, DC, 1978, p. 21.

[6]Seraudie, A., Blanchard, A., and Dor, J. B., "Qualification d'Essais en Ambiance Cryogenique a la Soufflerie T2," Association Aeronautique et Astronautique de France, Note Technique 86-07, Paris, Nov. 1986.

[7]Tobler, R. L., "Materials for Cryogenic Wind Tunnel Testing," National Bureau of Standards, NBSIR 79-1624, Washington, DC, May 1980.

[8]Lynch, F. T., and Patel, D. R., "Some Important New Instrumentation and Testing Requirements for Testing in a Cryogenic Wind Tunnel Such as the NTF," AIAA Paper 82-0605, March 1982, pp. 8, 9.

[9]Smith, W. J., *Modern Optical Engineering,* McGraw-Hill, New York, 1966, pp. 188–192.